DOI: 10.61782/fa.2023.0329

forum acusticum 2023

AEROACOUSTIC STUDY OF A TWIN-TURBOPROP AIRCRAFT USING THE LATTICE-BOLTZMANN METHOD

Edoardo Grande[1*] **Clelia Massarino**[1] **Florian Kroemer**[1]
Andreas Feigel[1] **Carlo Aquilini**[1]
[1] Airbus Defence and Space GmbH, Rechliner Straße, Manching 85077, Germany

ABSTRACT

The present study focuses on the prediction of ground-based tonal noise generated by a twin-turboprop aircraft in cruise flight at different heights, by means of a CFD/CAA-based approach. The unsteady flow solution of the 1:1 scale model is obtained using the Lattice-Boltzmann/Very Large Eddy Simulation method. Numerical predictions are validated against fly-over noise measurements conducted on the entire aircraft. Microphones were positioned both parallel and perpendicular to the flight path, in order to capture the directivity of the aircraft noise. The far-field noise spectra, computed via the Ffowcs-Williams and Hawkings´ acoustic analogy applied to the propeller and airframe surfaces, show a good correspondence between the numerical and experimental results at the first and second blade passing frequencies, with a maximum difference of 2 dB. Furthermore, the on-ground noise footprints reveal that the employed method is able to capture the complex acoustic field generated by the propellers and its scattering on the airframe. The latter gives a significant contribution especially outside of the propeller plane, showing the need to simulate the whole configuration for an accurate estimation of the on-ground noise levels.

Keywords: *propellers, turboprop, aeroacoustics, power-flow*

**Corresponding author*: *edoardo.grande@airbus.com.*

1. INTRODUCTION

Nowadays, turboprop aircrafts are widely used for short to medium flights, because their higher propulsive efficiency with respect to jet aircraft. However, since European regulations aim to drastically reduce the acoustic footprint of flying aircraft by 2050 [1], the expansion of the turboprop market will be closely related to rotor noise reduction. Turboprops have an increased noise emission compared to turbofan aircraft. The sound spectrum is dominated by the propellers tonal components, which are also the main responsible for cabin noise, perceived by passengers as more annoying than engine noise [2]. Several authors [3–6] investigated the aeroacoustic characteristics of installed propeller configurations, namely propeller-engine-wing. They showed that unsteady simulations are needed to capture the complex acoustic field generated by the propeller-airframe interaction and the importance of including the fuselage scattering for an accurate prediction of the noise levels. The acoustics of a full turboprop aircraft with different propeller installation layouts, i.e. co-rotating and counter-rotating with and without synchrophasing, is studied by Chirico et al. [7]. One of the main outcome is that the counter rotating top-in configuration is able to reduce the noise emissions.

In this paper the tonal noise generated by a twin-turboprop Beechcraft King Air 350 aircraft is predicted by means of high-fidelity simulations. The aircraft is flying in cruise conditions at two different altitudes, namely 760 ft and 5620 ft. On-ground noise measurements during a flight-test campaign with the full-scale aircraft configuration are performed. The aim of the study is twofold: first, to validate the tonal noise prediction tool-chain against the in-flight noise measurements and second, to exploit the numerical predictions to study the characteristics of

the on-ground noise field generated by the interactions of the propellers sound field among each other and the fuselage. The study of the broadband noise component is out of the scope of this work. The Lattice-Boltzmann/Very-Large Eddy Simulation (LB/VLES) method is employed to simulate the flow around the rotor. The aerodynamic noise generation is estimated by using an acoustic analogy based on Farassat's formulation 1A of the Ffowcs-Williams and Hawkings' (FW-H) equation.

The paper is organized as follows. In Sec. 2 the in-flight noise measurements campaign is presented. In Sec. 3 the computational methodology is described together with the computational setup and operating conditions. In Sec. 4 the noise spectra and on-ground noise footprints are discussed. The main findings and future work are presented in Sec. 5.

2. FLIGHT-TEST CAMPAIGN

On-ground noise measurements are conducted during a flight-test campaign at Cochstedt airport (Germany) with a Beechcraft King Air 350, a twin-turboprop aircraft with a wingspan b of 17.3 m, a length L of 14 m and a maximum capacity of 11 passengers (Fig. 1). The aircraft is equipped with two 5-bladed MTV-27 propellers with a diameter D = 2.6 m, rotating both counterclockwise as viewed from the front.

The flight-tests are conducted with the aircraft in cruise flight and cover a total of 15 testpoints, which are distinct by the aircraft´s altitude and speed as well as by the propeller RPM. Each testpoint is repeated up to four times. The aircraft is equipped with a GPS sensor. Flight parameters, such as propellers rotational speed, torque and fuel flow, are taken from cockpit readings. The thrust generated by the propellers is calculated by means of the engine performance model. During the tests, the air around the aircraft was unstable and turbulent, causing a speed variation of about 3-8 kts, an altitude variation of 20-60 ft and fluctuations in the torque reading between 0.5% and 1%. Fuel flow and propeller rotational speed showed stable readings.

A total of 11 microphones on-ground (see Fig. 2) are used, of which 7 of them are placed along the runway central line (green mics) and 4 of them at the beginning of the runway, with a lateral offset of 80 m (2 red mics) and 170 m (2 violet mics). Microphone signals are recorded for the full aircraft trajectory, with a sampling frequency of 48 kHz. Pressure spectra are calculated using a Hanning window and a frequency resolution of 3.125 Hz.

In order to compare the experimental results with the quasi-static high-fidelity simulations, the Doppler effect due to the source movement needs to be minimized. To achieve this, the section of the measured microphone pressure signals when the aircraft is above the respective microphone is selected, which results in a tailored time frame where the Doppler effect is significantly reduced.

Figure 1: Beechcraft King Air 350 at Cochstedt Airport.

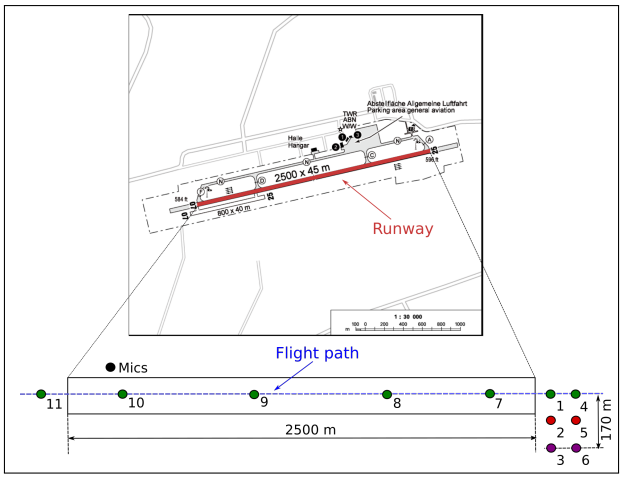

Figure 2: Microphones setup during the flight-test campaign at Cochstedt airport.

3. COMPUTATIONAL METHODOLOGY AND SETUP

3.1 Numerical method

The CFD/CAA solver Simulia PowerFLOW 6-2021-R3, based on the Lattice-Boltzmann Method (LBM), is used in this work to compute the flow around the aircraft and to predict the generated noise. Referring to aeroacoustics of rotating parts, this software has already been validated for UAV rotors [8–10], aircraft propellers [11] and aero engine fan/OGV stages [12, 13].

The LBM method solves the discrete form of the Boltzmann equation for the particle distribution function, which represents the probability of finding a particle at a spatial coordinate $\mathbf{x}$ and time t, while having a velocity $\mathbf{v}$. The solution of the Boltzmann equation is discretized onto a Cartesian mesh made of cubic volumetric elements (voxels). The surface of solid bodies is discretized within each voxel intersecting the wall geometry using planar surface elements (surfels). The discretization used for this particular application consists of 19 discrete velocities in three dimensions (D3Q19), involving a third-order truncation of the Chapman-Enskog expansion [14].

A Very Large Eddy Simulation (VLES) model is implemented to take into account the effect of the sub-grid unresolved scales of turbulence. Following [15], a two-equations $k-\epsilon$ renormalization group is used to compute a turbulent relaxation time that is added to the viscous relaxation time. To reduce the computational cost, a pressure-gradient-extended wall-model is used to approximate the no-slip boundary condition on solid walls [16, 17]. In order to simulate a rotating geometry, a ground-fixed reference frame is used in combination with a body-fixed Local Reference Frame (LRF). The LRF is characterized by a mesh that rigidly rotates with the rotating geometry so that no relative motion between the LRF grid and the enclosed geometry occurs.

Far-field noise is computed by using the Ffowcs-Williams and Hawkings (FW-H) acoustic analogy. The FW-H solver is based on a forward-time solution [18] of the formulation 1A of [19] extended to a convective wave equation [20].

3.2 Computational setup

The numerical simulations are conducted on the whole aircraft without active control surfaces and engine core. Two different cruise conditions, corresponding to testpoint 1 (TP 1) and 3 (TP 3) of the flight-test campaign, are simulated. The main flight parameters for these two testpoints are summarized in Tab. 1, where V is the indicated air speed in Knots, ALT is the cruise altitude in ft, ω the propellers rotational speed in rev/min and T_{SP} is the required thrust for the single propeller in N. The listed thrust is matched with a margin of 3% by adjusting the propeller collective pitch angle.

Table 1: Cruise operating conditions.

	V (KIAS)	ALT (ft)	ω (rpm)	T_{SP} (N)
TP 1	190	760	1500	2646
TP 3	182.5	5620	1500	2712

The computational fluid domain, sketched in Fig. 3, is a cubic volume of 65 L with the aircraft geometry at the center. Free-stream static pressure and velocity are prescribed on the domain boundary and a mass-flow rate is prescribed at the engine inlet and outlet. A total of 16 Variable Resolution (VR) regions are used to discretize the whole fluid domain, with the finest resolution region (VR16) placed around the blades leading edge, trailing edge and tip. The smallest voxel size is 0.8 mm, resulting in about 220 voxels along the mean chord. The resulting number of fine equivalent voxels for the current study is 45 million. An acoustic sponge, centered around the aircraft, is used to dissipate the acoustic waves and minimize the reflections from the external boundaries. The two propellers are encompassed by two rotating sliding meshes that define the Local Reference Frames (LRF), used to reproduce the propellers rotations.

The aeroacoustic analysis is performed by using the solid formulation of the FW-H analogy. The pressure fluctuations are sampled on the propeller blades and fuselage surfaces separately and the total noise level is obtained by summing up the energy from each source incoherently. Far-field noise is computed on ground, by distributing a total of 441 microphones in a squared area of 10 x 10 km. The aircraft is positioned at the center of this area and the ground is considered fully reflective. To compare the results with the measurements, the microphone positioned below the propeller plane, at the center between the two propellers, is used.

The simulation time is 0.48 sec, which corresponds to a total of 12 rotors revolutions. Acoustic data are sampled after 2 transient rotations, for 10 rotations (0.4 sec)

at a sampling frequency of 5 KHz. Power spectral density spectra are then calculated using the same spectral parameters as specified in Sec. 2 to ensure consistency in the successive comparison of the results.

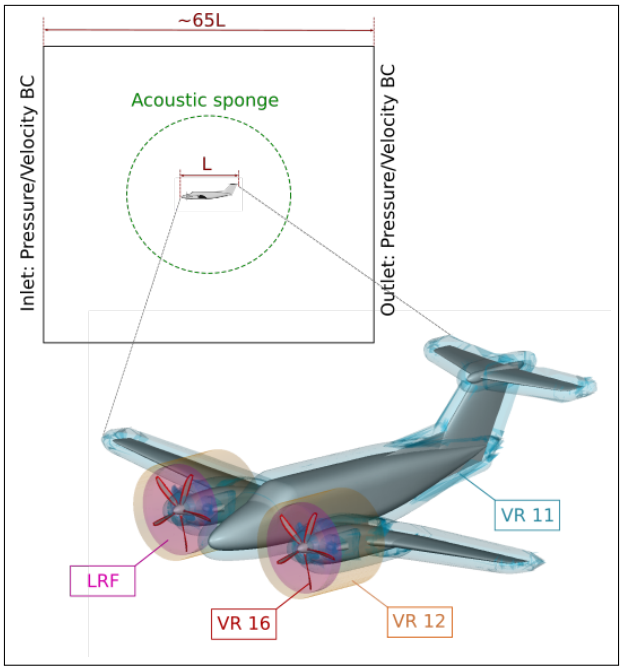

Figure 3: Sketch of the computational setup (not drawn to scale) with a zoom on the aircraft model.

4. RESULTS

4.1 Noise spectra

Figures 4 and 5 show a comparison between experimental and numerical noise spectra for TP 1 and 3, respectively. The experimental spectra are computed by averaging in the frequency domain the pressure signals from all the microphones placed along the runway central line (green dots in Fig. 2). The results from the lateral microphones (red and violet dots in Fig. 2) exhibit a similar behaviour, hence are not shown. The frequency axis of each plot is normalized with respect to the blade passing frequency $BPF = Bn$, where B is the number of blades and n is the propeller rotational frequency in Hz.

Due to the propellers rotation, the spectra present clear tones occurring at multiples of the first BPF, which dominate the noise content. The adopted method successfully predict the propellers tonal noise; in particular for TP 1, the tone at BPF 1 (125 Hz) and BPF 2 (250 Hz) are predicted within 2 dB difference with respect to the measurements. For TP3, the tones at BPF 1 and 2 match well with the measurements with a difference of about 1 dB. The BPF 3 (375 Hz) tone is covered from other noise sources in the experimental spectra, hence it is not possible to establish a reliable comparison with the numerical predictions. The fuselage scattering gives most of the contribution at BPF 1 and 2, with an SPL between 3 and 4 dB lower than the level due to propellers only.

As stated in the introduction, the analysis of the broadband noise is out of the scope of the present work. However, it is worth to mention that the higher broadband level in the measurements is due, on the one side, to airframe and engine core noise sources, which are not included in the computational setup and, on the other side, to the airport background noise, which plays a role especially at low frequencies.

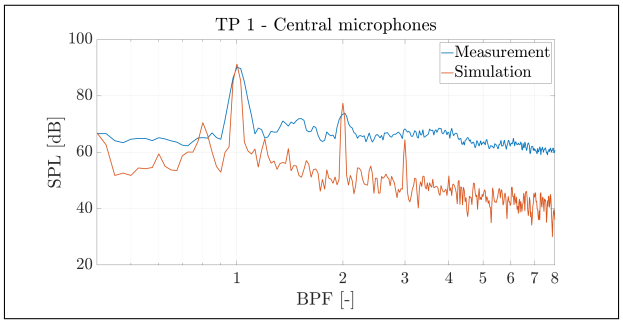

Figure 4: Comparison between experimental and numerical noise spectra for testpoint 1.

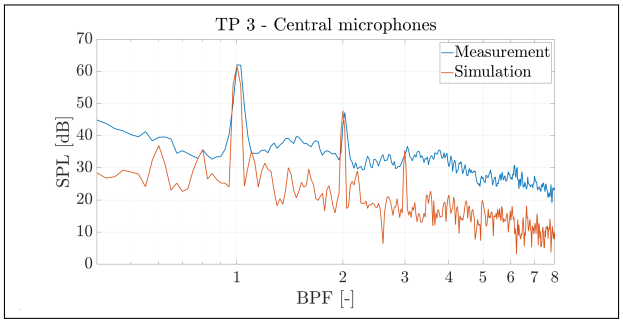

Figure 5: Comparison between experimental and numerical noise spectra for testpoint 3.

4.1.1 *Measurements variability*

The noise measurements are affected by uncertainty, which translate into a variability of the final noise spectra when the results from different microphones are compared. As mentioned in Sec. 2, the cruise flights were affected by wind gusts which caused variations in flight speed and altitude and fluctuations in the torque reading. Furthermore, from the GPS data, a lateral deviation of the aircraft trajectory between 16 ft and 50 ft, is observed. Finally, a variation of the angle of attack perceived by the propellers and an asymmetry of flow conditions between left and right propellers might be expected.

To quantify the variability of the noise spectra, the maximum and minimum SPL levels are extracted from the microphones placed along the runway central line. The results are plotted in Figs. 6 and 7 together with the numerical predictions, for TP 1 and 3, respectively. For TP1, a variation of about 3 dB at BPF 1 and 4 dB at the BPF 2 are observed; on the other hand, the variation for TP3 is higher and it is equal to about 8 dB and 7 dB at BPF 1 and 3. The numerical predictions for TP 1 are closer to the maximum measured values, while for TP 3 they lie in between the maximum and minimum experimental SPL levels.

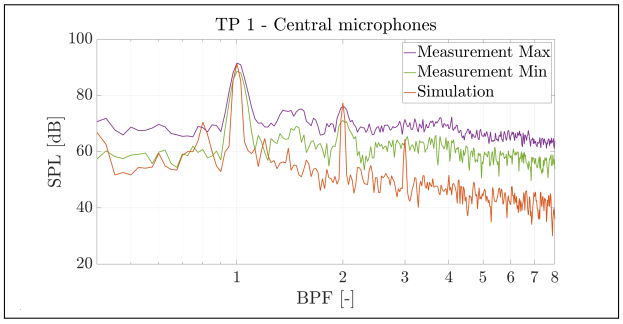

Figure 6: Noise measurements variability for testpoint 1

4.2 Noise footprints

Figs. 8 and 9 show the contributions of propellers and fuselage on the overall sound pressure level (OASPL) on ground (in an area of 10 x 10 km). For the sake of conciseness, only the results for TP 3 are presented. The noise from the propellers (see. Fig. 8) is driven by the loading noise directivity, i.e. it is predominant in the propellers rotational plane, with a maximum of 60 dB below the aircraft, and substantially reduces outside the plane. Similarly, the footprint due to fuselage scattering (see Fig. 9) also exhibits its maximum in the position below the aircraft with levels comparable with propeller noise. Furthermore, a significant noise level between 30 dB and 40 dB can be observed in all the other directions. This demonstrates the need to simulate the whole configuration to achieve an accurate noise estimation of a full aircraft in flight.

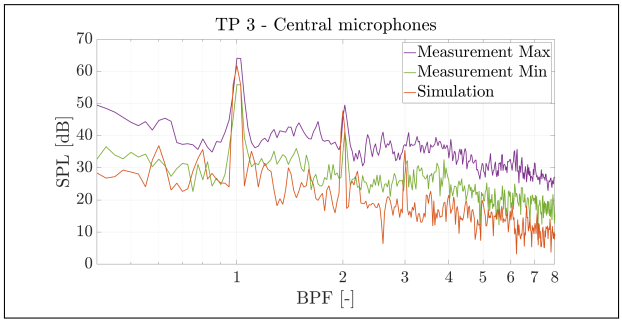

Figure 7: Noise measurements variability for testpoint 3

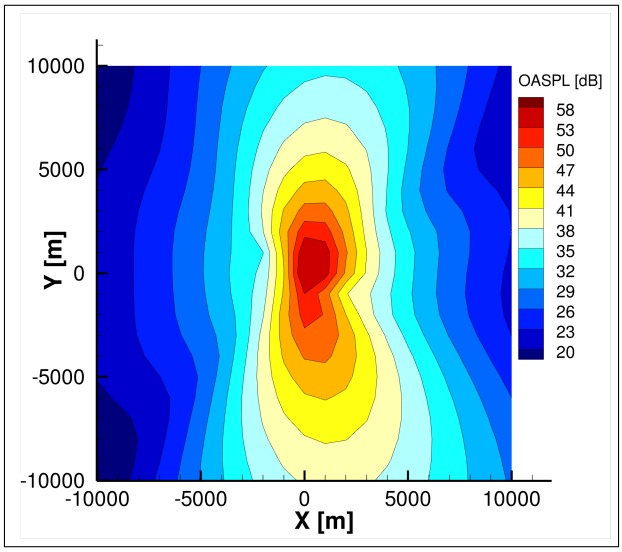

Figure 8: On-ground noise footprint for TP3: propellers contribution

Finally, it can be noticed that both propellers and fuselage acoustic fields are slightly asymmetric in the y direction, showing higher noise levels at negative y co-

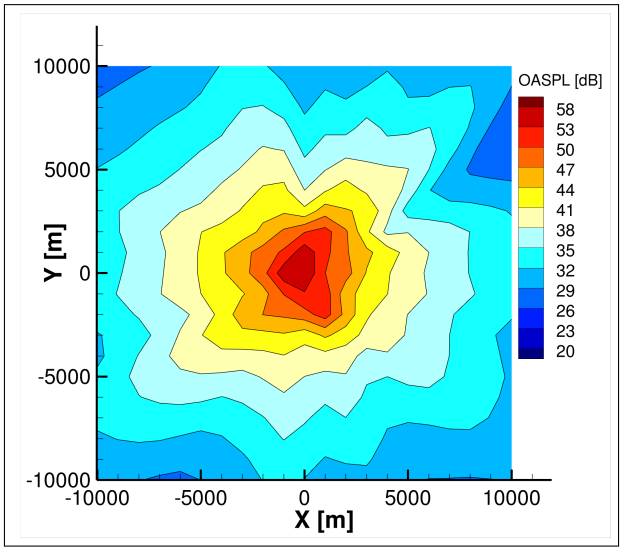

Figure 9: On-ground noise footprint for TP3: fuselage contribution

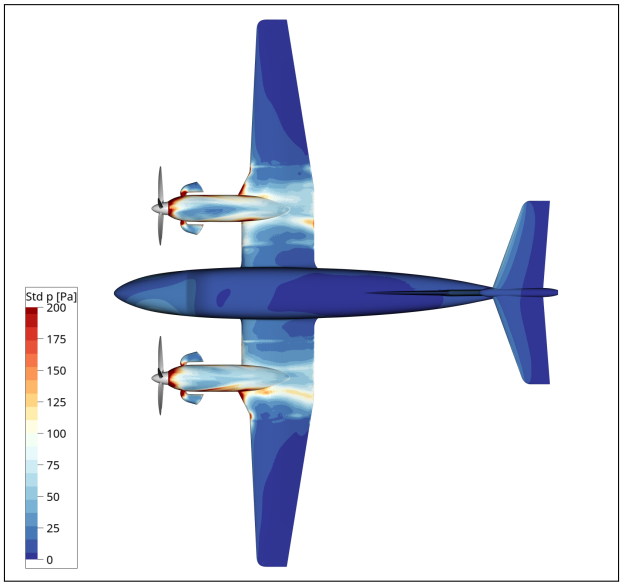

Figure 10: Standard deviation of surface pressure for TP 3.

ordinates. Indeed, the interaction of the propellers with the fuselage is not symmetric because one propeller approaches the fuselage when moving downwards and the other propeller when moving upwards. This causes an asymmetry in the propellers blade loading and tip vortex, thus a difference in the propellers tonal noise and in the pressure fluctuations generated by the interaction of the blade tip vortices with the wing. The unsteady pressure distribution on the aircraft surface is shown in Fig. 10. The footprint of the propellers tip vortex can be seen on the wings, with an higher level of pressure fluctuations on the left wing. A higher level of fluctuations on the left side of the aircraft nose (with respect to the right side), in proximity of the propeller plane, can also be noticed.

5. CONCLUSIONS

This paper presents a computational aeroacoustic study on a twin-turboprop aircraft Beechcraft King Air 350 in cruise conditions at two different altitudes (i.e. 760 ft and 5620 ft). The lattice Boltzmann method implemented in the CFD/CAA solver Simulia PowerFLOW is used to obtain the flow solution around the aircraft while the noise generation is computed by means of the Farassat's formulation 1A of the FW-H equation. The tonal noise predictions are validated against on-ground noise measurements conducted during flight tests with the entire aircraft.

The predicted noise spectra show a good agreement with the noise measurements. The tones at BPF 1 (125 Hz) and 2 (250 Hz) are predicted within 2 dB of accuracy for both testpoints. The experimental results show a low signal-to-noise ratio at BPF 3, hence a comparison with the numerical predictions cannot be established. The on-ground noise footprints show that the propellers noise is dominant in the propeller plane and that the contribution of the fuselage scattering needs to be considered. In particular, it results significant noise levels outside the propellers plane. Furthermore, the different interaction of the propellers with the fuselage (i.e. one propeller approaches the fuselage when moving upwards and the other when moving downwards) leads to slightly asymmetric footprints in the y direction.

Future works will include the calculation of the noise signatures over time at prescribed ground microphone locations by using an atmospheric propagation model based on a ray tracing method. The latter takes into account the aircraft trajectory and includes the effects of spherical spreading, atmospheric absorption, wind and temperature profile as well as Doppler shift.

6. ACKNOWLEDGMENTS

7. REFERENCES

[1] S. Kallas, M. Geoghegan-Quinn, M. Darecki, C. Edelstenne, T. Enders, E. Fernandez, and P. Hartman, "Flightpath 2050 europe's vision for aviation," *Report of the high level group on aviation research, European commission, Brussels, Belgium, Report No. EUR*, vol. 98, 2011.

[2] U. Emborg, F. Samuelsson, J. Holmgren, and S. Leth, "Active and passive noise control in practice on the saab 2000 high speed turboprop," in *4th AIAA/CEAS aeroacoustics conference*, p. 2231, 1998.

[3] C. Polacsek, P. Spiegel, F. Boyle, J. Eaton, H. Brouwer, and R. Nijboer, "Noise computation of high-speed propeller-driven aircraft," in *6th Aeroacoustics Conference and Exhibit*, p. 2086, 2000.

[4] J.-M. Bousquet and P. Gardarein, "Improvements on computations of high speed propeller unsteady aerodynamics," *Aerospace science and technology*, vol. 7, no. 6, pp. 465–472, 2003.

[5] A. Dumas and C. Castan, "Aerodynamic integration of high speed propeller on aircraft recent investigations in european wind tunnels," in *21st ICAS Congress, Melbourne (Australia)*, pp. 1–11, 1998.

[6] S. Leth, F. Samuelsson, and S. Meijer, "Propeller noise generation and its reduction on the saab 2000 high-speed turboprop," in *4th AIAA/CEAS Aeroacoustics Conference*, p. 2283, 1998.

[7] G. Chirico, G. N. Barakos, and N. Bown, "Propeller installation effects on turboprop aircraft acoustics," *Journal of Sound and Vibration*, vol. 424, pp. 238–262, 2018.

[8] D. Casalino, E. Grande, G. Romani, D. Ragni, and F. Avallone, "Definition of a benchmark for low reynolds number propeller aeroacoustics," *Aeroaspace Science and Technology*, 2021.

[9] G. Romani, E. Grande, F. Avallone, D. Ragni, and D. Casalino, "Performance and noise prediction of low-reynolds number propellers using the lattice-boltzmann method," *Aerospace Science and Technology*, p. 107086, 09 2021.

[10] G. Romani, E. Grande, F. Avallone, D. Ragni, and D. Casalino, "Computational study of flow incidence effects on the aeroacoustics of low blade-tip mach number propellers," *Aerospace Science and Technology*, vol. 120, p. 107275, 2022.

[11] F. Avallone, D. Casalino, and D. Ragni, "Impingement of a propeller-slipstream on a leading edge with a flow-permeable insert: A computational aeroacoustic study," *International Journal of Aeroacoustics*, vol. 17, no. 6-8, pp. 687–711, 2018.

[12] F. Avallone, L. Ende, Q. Li, D. Ragni, D. Casalino, G. Eitelberg, and L. Veldhuis, "Aerodynamic and aeroacoustic effects of swirl recovery vanes length," *Journal of Aircraft*, 08 2019.

[13] I. Gonzalez-Martino and D. Casalino, "Fan tonal and broadband noise simulations at transonic operating conditions using lattice-boltzmann methods," in *2018 AIAA/CEAS aeroacoustics conference*, p. 3919, 2018.

[14] H. Chen, S. Chen, and W. Matthaeus, "Recovery of the Navier-Stokes equations using a lattice-gas Boltzmann method," *Physical Review A*, vol. 45, pp. R5339–R5342, 4 1992.

[15] V. Yakhot and S. Orszag, "Renormalization group analysis of turbulence. I. Basic theory," *Journal of Scientific Computing*, vol. 1, no. 1, pp. 3–51, 1986.

[16] C. Teixeira, "Incorporating Turbulence Models into the Lattice-Boltzmann Method," *International Journal of Modern Physics C*, vol. 09, pp. 1159–1175, 12 1998.

[17] D. Wilcox, *Turbulence modelling for CFD (Third Edition)*. DCW Industries, Incorporated, 2006.

[18] D. Casalino, "An advanced time approach for acoustic analogy predictions," *Journal of Sound and Vibration*, vol. 261, no. 4, pp. 583–612, 2003.

[19] F. Farassat and G. P. Succi, "A review of propeller discrete frequency noise prediction technology with emphasis on two current methods for time domain calculations," *Journal of Sound and Vibration*, vol. 71, no. 3, pp. 399–419, 1980.

[20] G. Brès, F. Pérot, and D. Freed, "Properties of the lattice boltzmann method for acoustics," in *15th AIAA/CEAS Aeroacoustics Conference (30th AIAA Aeroacoustics Conference)*, p. 3395, 2009.